Triggering of El Niño onset through trade wind–induced charging of the equatorial Pacific

Bruce T. Anderson,[1] Renellys C. Perez,[2] and Alicia Karspeck[3]

Received 5 December 2012; accepted 25 January 2013; published 25 March 2013.

[1] Sea surface temperature variations over the equatorial Pacific associated with the El Niño/Southern Oscillation (ENSO) produce changes in climates across the globe. Here we report evidence from observationally constrained ocean data for the initiation of warm ENSO events (El Niños) resulting from subsurface equatorial Pacific heat content increases related to tropical/extratropical sea level pressure (SLP) changes over the North Pacific. We hypothesize that the increase in heat content is a response to SLP-generated variations in the North Pacific trade winds, which we term trade wind charging of the equatorial Pacific. Experiments using a high-resolution numerical ocean model verify that the charging of subsurface heat content along the equatorial Pacific can be induced by SLP-generated trade wind variations. Furthermore, analysis of the numerical model results and historical observations indicates that the trade wind–induced ocean heat content increases are sufficiently large to initiate the onset of El Niño events, which mature approximately 12 months after the trade wind forcing itself.
Citation: Anderson, B. T., R. C. Perez and A. Karspeck (2013), Triggering of El Niño onset through trade wind–induced charging of the equatorial Pacific, *Geophys. Res. Lett.*, *40*, 1212–1216, doi:10.1002/grl.50200.

1. Introduction

[2] The El Niño/Southern Oscillation (ENSO) imposes changes to regional climates across the globe, with significant physical, biological, and socioeconomic impacts [*Bradley et al.*, 1987; *Francey et al.*, 1995; *Stenseth et al.*, 2002; *Schubert et al.*, 2004; *Behrenfeld et al.*, 2006; *Hsiang et al.*, 2011]. Previous research [*Trenberth and Shea*, 1987; *Barnett et al.*, 1988; *Vimont et al.*, 2003; *Anderson*, 2003] has shown that variations in the ENSO—here characterized by the Niño-3 index, which captures the largest ENSO-related sea surface temperature (SST) departures [*Rasmusson and Carpenter*, 1982; *Philander*, 1983]—during its season of maximum variance (e.g., November–January) [*Trenberth*, 1997; *Jin et al.*, 1994]—are preceded by a mode of sea level pressure (SLP) and wind stress variability in the central tropical/extratropical North Pacific approximately 12 months earlier (Figure 1).

[3] As highlighted by others [*Vimont et al.*, 2009; *Di Lorenzo et al.*, 2010], the pattern of preceding SLPs (Figure 1a) is characteristic of the positive phase of the North Pacific Oscillation [*Walker and Bliss*, 1932; *Rogers*, 1981; *Linkin and Nigam*, 2008], with significant negative SLP anomalies centered over the subtropical North Pacific that extend into the tropics and the Southern Hemisphere. A similar relationship is found when considering just those anomalies preceding El Niño (positive ENSO) events (Figure 1 in supporting material—hereafter, SM). This precursor pattern of SLP variability can be captured by a sea level pressure index (SLPI) centered on 175°W–140°W and 10°N–25°N [*Anderson*, 2003]. The seasonal mean value of the SLPI in boreal winter, defined here as November–March, has a significant negative correlation with the November–January ENSO state 12 months later (Figure 1b) such that negative boreal winter SLPI values can be significant predictors of El Niño events at lead times of around 1 year (Figure 1b in SM).

[4] In this study, we use observationally constrained ocean reanalysis data along with high-resolution numerical ocean model simulations to analyze the mechanism responsible for this statistical relationship. Previous evidence suggests that variations in the North Pacific trade winds, induced by the SLP anomalies, can directly force subsurface heat content changes across the central equatorial Pacific [*Anderson*, 2004; *Anderson and Maloney*, 2006], which serve as precursors to mature El Niño (warm ENSO) events [*Jin*, 1997; *Meinen and McPhaden*, 2000; *McPhaden*, 2003; *Newman et al.*, 2011]. Here we present the first process-based confirmation of this "trade wind charging" (TWC) hypothesis for initiating changes in the state of the equatorial Pacific.

2. Ocean Analysis

[5] The evolution of atmospheric and oceanic fields taken from the observationally constrained ORA-S3 European Centre for Medium-Range Weather Forecasts (ECMWF) ocean reanalysis [*Balmaseda et al.*, 2008]—including wind stress, SST, and oceanic heat content—concurrent with and following negative boreal winter SLPI values indicate significant weakening of the climatological northeasterly trade winds over most of the North Pacific basin, with a strengthening of the equatorial easterlies in the eastern portion of the basin during December–March (Figure 2). Initial (December) SST anomalies are found only over the central tropical and subtropical North Pacific, colocated with the overlying wind stress anomalies (Figure 2a). By January, positive SST anomalies form in the equatorial western Pacific (Figures 2b and 2c). At the same time, subsurface temperature anomalies develop in the central equatorial Pacific (between 180°W and 150°W) and over the central tropical North Pacific along 5°N (between 165°W and 135°W),

All Supporting Information may be found in the online version of this article.

[1]Department of Earth and Environment, Boston University, Boston, Massachusetts, USA.
[2]Cooperative Institute of Marine and Atmospheric Studies/University of Miami, NOAA/Atlantic Oceanographic and Meteorological Laboratory, Miami, Florida, USA.
[3]National Center for Atmospheric Research, Boulder, Colorado, USA.

Corresponding author: Bruce T. Anderson, Department of Earth and Environment, Boston University, 675 Commonwealth Ave., Boston, MA 02215, USA. (brucea@bu.edu)

0094-8276/13/10.1002/grl.50200

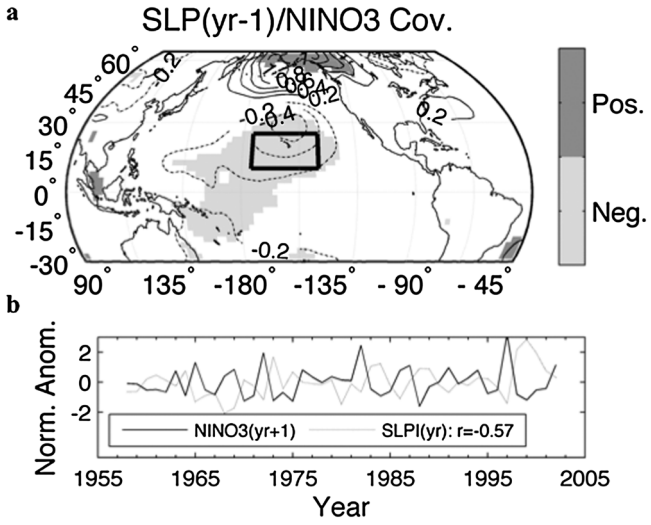

Figure 1. (a) Contour: Boreal winter (November–March) seasonal mean SLP anomalies, obtained from the European Center for Midrange Weather Forecasting (ECMWF) ERA-40 reanalysis [*Uppala et al*., 2005], regressed against the following year's November–January Niño-3 index at every grid point in the Pacific from 1958 to 2001. Minimum contour is ±0.2 hPa; contour interval is 0.2 hPa. Shading: Regression values that exceed the 90% significance level, based on a two-tailed *T* test. The black box indicates the averaging region for the SLPI, which is constructed by calculating the monthly grid point SLP anomalies with respect to the climatological value for the given month and then normalizing these grid point anomalies by their interannual standard deviation. The normalized monthly anomalies are then area-averaged over the region in the box (175°W–140°W, 10°N–25°N) to arrive at monthly values for the SLPI. (b) The time series of normalized boreal winter seasonal mean SLPI anomalies (dashed line) plotted with respect to the January date (i.e., the first value represents November 1957 to March 1958). Also shown is the time series of the normalized November–January Niño-3 index (solid line) shifted forward 1 year (i.e., the first value represents November 1958 to January 1959).

consistent with the TWC hypothesis [cf. *Anderson*, 2004; *Anderson and Maloney*, 2006].

[6] During late boreal winter (February–March), the initial SST anomalies, stretching from the western equatorial Pacific into the central tropical and subtropical North Pacific, intensify (Figures 2d–2g). However, their position remains relatively stationary despite significant zonal wind stress anomalies to the south, suggesting that the SST anomalies are not changing in response to surface fluxes along the equatorward edge of the wind stress anomaly field. Instead the southernmost zonal wind stress anomalies are colocated with a strengthening of off-equatorial central Pacific temperature anomalies in the subsurface, which exceed those in the equatorial region. Vertical cross sections through these surface and subsurface temperature anomalies indicate that the largest subsurface off-equatorial warming is occurring along the thermocline near 3°N in the region of climatological warm water generated by the tropical cell circulation north of the Equator (Figures 2d–2g in SM), while surface warming is confined to regions north of 10°N.

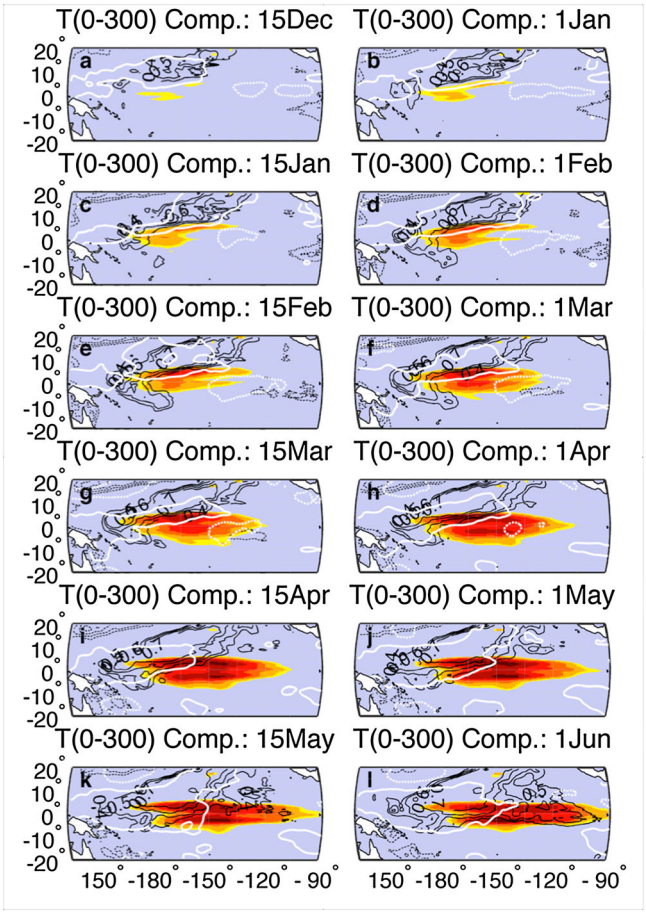

Figure 2. The evolution of the tropical Pacific ocean/atmosphere system concurrent with and following atmospheric variability in the SLPI region. Shading: Composite of normalized monthly-mean heat content anomalies, represented by the vertically averaged temperature anomalies integrated from 0 to 300m. Shading interval is from 0.4 (yellow) to 1.0 (maroon) in increments of 0.1; for clarity only positive values that exceed the 90% significance level are shown (>0.44). Black contours: Composite of normalized monthly mean near-surface temperature anomalies at 5 m depth. Contour interval is 0.1; minimum contour is ±0.4. White contours: Composite of normalized monthly mean zonal wind stress anomalies. For clarity, only the boundary of significant (90% confidence) anomalies are shown. Positive (negative) values have solid (dashed) contours. For compositing, all anomalies are normalized by their interannual standard deviations and then a weighted average is performed using the normalized SLPI values for years in which the mean November–March SLPI is negative (which comprise 24 of the 44 years). Significance determined using a boot strap analysis in which the same method is applied to 10,000 sets of 44 normally distributed random predictor/predictand values. Data taken from the ECMWF ocean reanalysis system (ORA-S3). Panels—starting 15 December concurrent with the November–March SLPI (a) and extending through 1 June (l)—show 30 day mean values centered on the given date; to obtain higher frequency resolution, intermediate fields are based on a simple linear interpolation of the corresponding monthly mean values.

[7] During April, the SST anomalies in the central portion of the basin begin to shift equatorward (Figures 2 h and 2i).

Concurrently, the subsurface temperature anomalies south of the equator intensify and convolve with the equatorial and off-equatorial anomalies to the north, forming a nearly symmetric, extensive subsurface temperature anomaly spanning 180°W–120°W and 5°S–5°N representative of a charging of the warm water volume of the equatorial Pacific that serves as a precursor to mature El Niño events [*Meinen and McPhaden*, 2000; *McPhaden*, 2003; *Newman et al.*, 2011]. During April and through June, the subsurface temperature anomaly expands eastward, reaching the eastern portion of the basin approximately a month before the SST anomalies themselves (cf. Figures 2j and 2l). In addition, the zonal wind stress anomalies shift south and become more symmetric about the equator. By June, positive SST anomalies are found across the tropical Pacific basin (Figure 2l). Over the next few months, these anomalies intensify, generating a characteristic El Niño–type pattern by the end of the calendar year (Figure 3 in SM).

3. Numerical Simulation of TWC

[8] To ascertain the importance of TWC in generating the surface and subsurface temperature evolution of the ocean, the wind stress and heat flux anomaly fields during the middle of boreal winter are composited for years with negative SLPI values (based on a weighted average of the values during those years; Figure 4, left, in SM). These anomaly fields are then used to force a high-resolution dynamical ocean model [*Perez and Kessler*, 2009] centered on the equatorial Pacific basin, using a ramp-up/ramp-down technique in which the full forcing fields are added to the climatological fields and persisted for the period December–March (Figure 4f in SM). The ocean model is then allowed to evolve over the next 3 months with only climatological forcing.

[9] The model response to the imposed forcing is consistent with the composite analysis detailed above. Subsurface temperature anomalies first develop along the off-equatorial central North Pacific in mid-December (Movie 1 in SM). As these intensify, additional subsurface anomalies form over the equatorial Pacific near the date line as well as in the off-equatorial central South Pacific. Subsequently, the equatorial and near-equatorial subsurface temperature anomalies strengthen and propagate eastward along the thermocline, shoaling and reaching the eastern equatorial Pacific by 1 March, when they start to warm the surface waters. After the cessation of wind stress and heat flux forcing at the end of March, the subsurface temperature anomalies associated with TWC begin to dissipate; however, their continued eastward propagation along the thermocline results in an intensification of the SST anomalies through May and June, setting the stage for the onset of an El Niño event.

[10] Sensitivity experiments designed to isolate the influence of (1) western equatorial Pacific wind stress anomalies, (2) central equatorial and off-equatorial Pacific wind stress anomalies, and (3) heat flux anomalies (Figure 4 in SM) highlight the important role of central Pacific wind stress

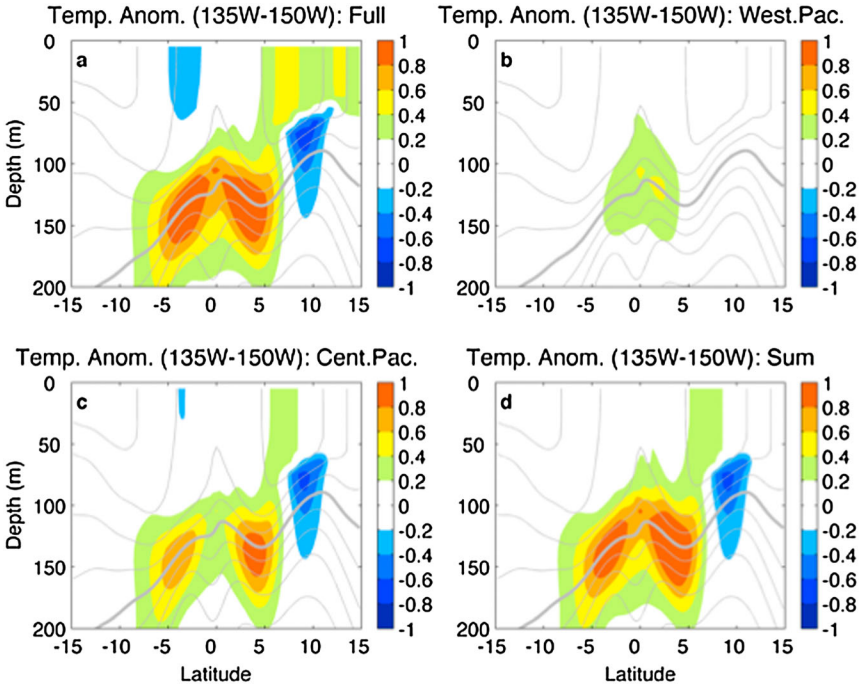

Figure 3. Subsurface temperature anomalies across the central Pacific Ocean that develop in response to idealized wind stress and heat flux forcing of the ocean system. (a) Shading: Difference in 3 month mean (1 January to 31 March) temperature values, averaged over 150°W–135°W, derived from (i) three simulations with wind stress and heat flux anomalies (shown in Figure 4 in SM) applied to the seasonally varying climatological fields and (ii) three simulations with the seasonally varying climatological forcing fields only, plotted with latitude (*X* axis) and depth (*Y* axis). Shading interval is 0.2°C; minimum contour is ±0.2°C. Gray contours: 3 month mean isotherms taken from the control simulations. Contour interval is 2°C; for reference, the 22°C isotherm is indicated by the heavy, gray contour. The other three panels show 3 month mean (1 January to 31 March) temperature anomalies induced by (b) western equatorial Pacific wind stress anomalies only; (c) central Pacific wind stress anomalies only; and (d) the sum of the temperature anomalies induced by the western equatorial Pacific and central Pacific wind stress anomalies separately.

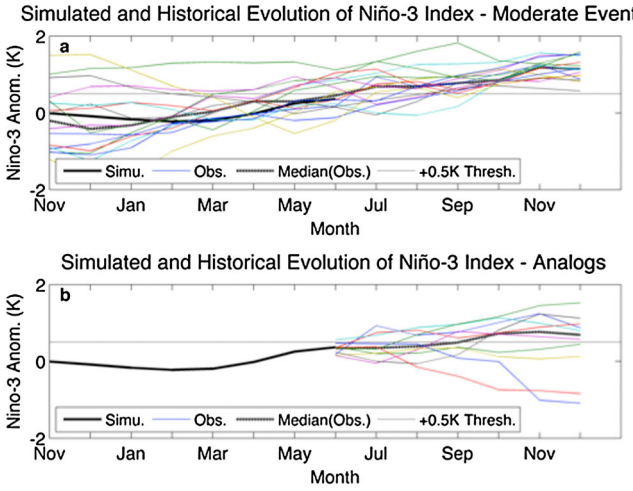

Figure 4. The evolution of the ENSO system in response to wind stress and heat flux forcing of the ocean system. Solid black line: The simulated Niño-3 index anomaly derived from the difference between (i) three simulations with wind stress and heat flux anomalies (shown in Figure 4 in SM) applied to the seasonally varying climatological fields and (ii) three simulations with the seasonally varying climatological forcing fields only. Thin lines: the observed Niño-3 index anomaly. Dashed black line: the median observed Niño-3 index anomaly. Gray horizontal line: 0.5 K anomaly value designating El Niño conditions in the eastern equatorial Pacific. (a) Observed Niño-3 index for all years leading up to a moderate El Niño during the October–December period, as designated by a 3 month mean value greater than 0.5 K but less than 2.0 K, which excludes the three intense El Niños of 1972/1973 (+2.2 K), 1982/1983 (+2.8 K), and 1997/1998 (+3.4 K). Values plotted from November of the prior year through to December of the current year. (b) Observed Niño-3 index for all years that are analogous to the simulated evolution for the period January–June. Analogous years are defined as ones in which (i) the linear trend of the observed Niño-3 index is positive from January to June and (ii) the June value of the observed Niño-3 index lies within ±0.25K of the simulated value during June. Analogous years plotted from June to December of the current year.

forcing in initiating off-equatorial as well as equatorial subsurface temperature anomalies associated with TWC (Figure 3). Furthermore, these sensitivity experiments reveal that surface heat flux forcing principally influences the tropical SSTs in the region of weakening trade winds but in the absence of any coupling with the overlying atmosphere (which is treated more fully in *Vimont et al*. [2001], *Vimont et al*. [2003], *Alexander et al*. [2010]) surface heat flux forcing has little influence on the subsurface temperature anomalies or on the subsequent emergence of SST anomalies in the eastern equatorial Pacific (Movie 2 in SM).

[11] Instead, the positive SST anomalies that develop over the eastern equatorial Pacific (Figure 5 in SM) are initially (from approximately 1 April to 1 June) a response to the shoaling of subsurface temperature anomalies initiated by western Pacific wind stress forcing (Movie 2 in SM), which propagate to the eastern equatorial Pacific as Kelvin waves [*McCreary*, 1976]. As the surface temperature anomaly signature of the western Pacific forcing begins to dissipate (June 1), the eastern equatorial Pacific SST anomalies are sustained and augmented by the shoaling of off-equatorial and equatorial subsurface temperature anomalies induced by central Pacific wind stress forcing (Movie 2 in SM)—the result of negative wind stress curl anomalies at 5°N (as well as positive wind stress curl anomalies at 5°S), which tend to produce a charging of the thermocline via equatorward vertically integrated mass transport as well as vortex stretching [cf. *Clarke et al*., 2007]—such that by the end of the integration the SST anomalies exceed 0.5 °C over a broad region of the eastern equatorial Pacific (Figure 5l in SM).

[12] As noted before, similar surface temperature features—including the initial warm anomalies in the central tropical North Pacific and the subsequent emergence and intensification of warm anomalies in the eastern equatorial Pacific—are found in the observationally constrained ocean reanalysis as well (Figure 6 in SM). Indeed, a comparison of SST anomalies in the eastern equatorial Pacific at the end of the numerical model integration, as characterized by the Niño-3 index, with those found in the historical record at the same time of year indicates that the wind stress–induced SST anomalies are (a) consistent with ones that develop into mature El Niño events over the course of the subsequent 4–6 months and (b) likely to evolve into mature El Niños over the course of the subsequent 4–6 months (Figure 4), even absent further equatorial wind stress forcing over the western Pacific during the May–June period.

4. Summary

[13] Observational evidence suggests that El Niños (in contrast to La Niñas) may require an initiation of subsurface warming across the Pacific basin distinct from that supplied by the system's oscillatory dynamics [*Kessler*, 2002]. Here we show that such initiation can be triggered through the wind stress–induced modification of the subsurface equatorial Pacific ocean temperatures via trade wind charging of the equatorial Pacific, a process driven by tropical/extratropical SLP changes over the North Pacific. In our study, we find no evidence that these SLP changes are related to the concurrent or preceding ENSO cycle (Figure 7 in SM). We emphasize that the mechanism outlined here is fundamentally different from previous ones investigating extratropical atmospheric forcing of the tropical Pacific. These include the oscillatory modification of the equatorial Pacific warm water volume associated with recharge/discharge mechanisms, which given the weakening of the trade winds analyzed here would produce a discharge of warm water from the equatorial Pacific [*Jin*, 1997]; the equatorward shift of atmospheric circulations induced by the seasonal persistence of subtropical SST anomalies associated with the Seasonal Footprinting Mechanism, which does not influence the structure of the subsurface equatorial Pacific until the following boreal spring [*Vimont et al*., 2001; *Vimont et al*., 2003]; trade wind–induced variations in evaporation associated with the Meridional Mode, which to first order involves only the surface temperatures [*Alexander et al*., 2010]; and Rossby wave dynamics, which on short time scales (<12 months) involve the initiation and westward propagation of subsurface ocean anomalies distinct from those analyzed here (as evidenced by their geographic location—west of 170E° at latitudes between 20°N–30°N [*Solomon et al*., 2008]).

[14] The TWC mechanism elucidated here is not considered to be the sole initiator of ENSO events—other initiating mechanisms, including those listed above, can contribute to the onset of a particular event [*Neelin et al*., 1998]. However, these results do support the idea that precursor changes in North Pacific extratropical sea level pressures and central tropical Pacific trade winds play a role in El Niño initiation. Atmospheric variability in this region is in part related to internal variability of the extratropical Pacific storm track [*Linkin and Nigam*, 2008; *Caballero and Anderson*, 2009; *Riviere*, 2010] and as such is inherently unpredictable [*Di Lorenzo et al*., 2010]. However, it has also been linked to deterministic processes in the tropical Pacific on interannual [*Ashok and Yamagata*, 2009] to decadal time scales [*Di Lorenzo et al*., 2010], suggesting the potential for enhanced predictability of ENSO even prior to the 12–15 months studied here.

[15] **Acknowledgments.** This work was supported by the Department of Energy (DE-SC0004975 to B.T.A.). R.C.P. was supported by the NOAA/Atlantic Oceanographic and Meteorological Laboratory and the Cooperative Institute of Marine and Atmospheric Studies at the University of Miami. A.K. was supported by National Center for Atmospheric Research, which is sponsored by NSF. We also extend our thanks to Ekaterina Oleinik at Boston University's Scientific Computing and Visualization group for all her work in designing and producing the accompanying animations.

References

Alexander, M. A., D. J. Vimont, P. Chang, and J. D. Scott (2010), The impact of extratropical atmospheric variability on ENSO: Testing the seasonal footprinting mechanism using coupled model experiments. *J. Climate*, *23*, 2885–2901.

Anderson, B. T. (2003), Tropical Pacific sea-surface temperatures and preceding sea level pressure anomalies in the subtropical North Pacific. *J. Geophys. Res.*, *108*, doi:10.1029/2003JD003805.

Anderson, B. T. (2004), Investigation of a large-scale mode of ocean-atmosphere variability and its relation to tropical Pacific sea surface temperature anomalies. *J. Climate*, *17*, 1089–4098.

Anderson, B. T., and E. Maloney (2006), Interannual tropical Pacific sea surface temperatures and their relation to preceding sea level pressures in the NCAR CCSM2. *J. Climate*, *19*, 998–1012.

Ashok, K., and T. Yamagata (2009), The El Niño with a difference. *Nature*, *461*, 481–484.

Balmaseda, M. A., A. Vidard, and D. L. T. Anderson (2008), The ECMWF ocean analysis system: ORA-S3. *Mon. Wea. Rev.*, *136*, 3018-3034.

Barnett, T. et al. (1988), On the prediction of the El Niño of 1986-1987. *Science*, *241*, 92–196.

Behrenfeld, M. J. et al. (2006), Climate-driven trends in contemporary ocean productivity. *Nature*, *444*, 752–755.

Bradley, R. S., H. F. Diaz, G. N. Kiladis, and J. K. Eischeid (1987), ENSO signal in continental temperature and precipitation records. *Nature*, *327*, 497–501.

Caballero, R., and B. T. Anderson (2009), Impact of midlatitude stationary waves on regional Hadley cells and ENSO. *Geophys. Res. Lett.*, *36*, doi: 10.1029/2009GL039668.

Clarke, A. J., S. Van Gorder, and G. Colantuono (2007), Wind stress curl and ENSO discharge/recharge in the equatorial Pacific. *J. Phys. Oceanogr.*, *37*, 1077–1091.

Di Lorenzo, E. et al. (2010), Central Pacific El Niño and decadal climate change in the North Pacific Ocean. *Nat. Geosci.*, *3*, 762–765.

Francey, R. J. et al. (1995), Changes in oceanic and terrestrial carbon uptake since 1982. *Nature*, *373*, 326–330.

Hsiang, S. M., K. C. Meng, and M. A. Cane (2011), Civil conflicts are associated with global climate. *Nature*, *476*, 438–441.

Jin, F.-F. (1997) An equatorial ocean recharge paradigm for ENSO. 1. Conceptual model. *J. Atmos. Sci. 54*, 811–829.

Jin, F.-F., J. D. Neelin, and M. Ghil (1994), El Niño on the Devil's staircase – annual subharmonic steps to chaos. *Science*, *164*, 70–72.

Kessler, W. S. (2002), Is ENSO a cycle or a series of events? *Geophys. Res. Lett.*, *29*, doi:10.1029/2002GL015924.

Linkin, M. E., and S. Nigam (2008), The North Pacific Oscillation-West Pacific teleconnection pattern: Mature-phase structure and winter impacts. *J. Climate*, *21*, 1979–1997.

McCreary, J. (1976), Eastern tropical ocean response to changing wind systems – with application to El Niño. *J. Phys. Oceanogr.*, *6*, 632–645.

McPhaden, M. J. (2003), Tropical Pacific Ocean heat content variations and ENSO persistence barriers. *Geophys. Res. Lett.*, *30*, doi:10.1029/2003GL016872.

Meinen, C. S., and M. J. McPhaden (2000), Observations of warm water volume changes in the equatorial Pacific and their relationship to El Niño and La Niña. *J. Climate*, *13*, 3551–3559.

Neelin, J. D. et al. (1998), ENSO Theory. *J. Geophys. Res. 103*, 14261-14290.

Newman, M., M. A. Alexander, and J. D. Scott (2011), An empirical model of tropical ocean dynamics. *Clim. Dyn.*, *37*, 1823–1841.

Perez, R. C., and W. S. Kessler (2009), Three-dimensional structure of tropical cells in the central equatorial Pacific Ocean. *J. Phys. Oceanogr.*, *39*, 27–49.

Philander, S. G. H. (1983), El Niño Southern Oscillation phenomena. *Nature*, *302*, 295–301.

Rasmusson, E. M. and T. H. Carpenter (1982), Variations in tropical sea surface temperature and surface wind fields associated with the Southern Oscillation/El Niño. *Mon. Wea. Rev.*, *110*, 354–384.

Riviere, G. (2010), Role of Rossby wave breaking in the west Pacific teleconnection. *Geophys. Res. Lett.*, *37*, doi:10.1029/2010GL043309.

Rogers, J. C. (1981), The North Pacific Oscillation. *J. Climatol.*, *1*, 39–57.

Schubert, S. D. et al. (2004), On the cause of the 1930s Dust Bowl. *Science*, *303*, 1855–1859.

Solomon, A., S.-I. Shin, M. A. Alexander, and J. P. McCreary (2008), The relative importance of tropical variability forced from the North Pacific through ocean pathways. *Clim. Dyn.*, *31*, 315–331.

Stenseth, N. C. et al. (2002), Ecological effect of climate fluctuation. *Science*, *297*, 1292–1296.

Trenberth, K. E. (1997), The definition of El Niño. *Bull. Amer. Meteorol. Soc.*, *78*, 2771–2777.

Trenberth, K. E. and D. J. Shea (1987), On the evolution of the Southern Oscillation. *Mon. Wea. Rev.*, *115*, 3078-3096.

Uppala, S. M. et al. (2005), The ERA-40 re-analysis. *Quart. J. R. Meteorol. Soc.*, *131*, 2961–3012.

Vimont, D. J., S. Battisti, A. C. Hirst (2001), Footprinting: A seasonal connection between the tropics and mid-latitudes. *Geophys. Res. Lett.*, *28*, 3923–3926.

Vimont, D. J., S. Battisti, and A. C. Hirst (2003), The seasonal footprinting mechanism in the CSIRO general circulation models. *J. Climate*, *16*, 2653–2667.

Vimont, D. J., M. Alexander, and A. Fontaine (2009), Midlatitude excitation of tropical variability in the Pacific: The role of thermodynamic coupling and seasonality. *J. Climate*, *22*, 518–534.

Walker, G. T., and E. W. Bliss (1932), World Weather V. *Mem. R. Meteorol. Soc. 4*, 53–83.